Following De Novo Triglyceride Dynamics in Ovaries of Aedes Aegypti Mosquitoes

Lilian Valadares Tose
Florida International University
Chad R. Weisbrod
National High Magnetic Field Laboratory
Veronika Michalkova
Institute of Parasitology
Marcela Nouzova
Florida International University
Fernando G. Noriega
Florida International University
Francisco Fernandez-Lima (fernandf@fiu.edu)
Florida International University

Research Article

Keywords: egg development, hexapolar detection, Ultra-High Resolution Mass Spectrometry (UHRMS), PVG

Posted Date: February 13th, 2021

DOI: https://doi.org/10.21203/rs.3.rs-186208/v1

Abstract

Understanding the molecular and biochemical basis of egg development is a central topic in mosquito reproductive biology. Lipids are a major source of energy and building blocks for the developing ovarian follicles. Ultra-High Resolution Mass Spectrometry (UHRMS) combined with *in vivo* metabolic labeling of follicle lipids with deuterated water (^2H_2O) can provide unequivocal identification of *de novo* lipid species during ovarian development. In the present study, we followed *de novo* triglyceride (TG) dynamics during the ovarian previtellogenic (PVG) stage (2-7 days post-eclosion) of female adult *Aedes aegypti*. The incorporation of stable isotopes from the diet was evaluated using liquid chromatography (LC) in tandem with the high accuracy (<0.3 ppm) and high mass resolution (over 1M) of a 14.5 Tesla Fourier Transform Ion Cyclotron Resonance Mass Spectrometer (14.5 T FT-ICR MS) equipped with hexapolar detection. LC-UHRMS provides effective lipid class separation and chemical formula identification based on the isotopic fine structure. The monitoring of stable isotope incorporation into *de novo* incorporated TGs suggests that ovarian lipids are consumed or recycled during the PVG stage, with variable time dynamics. These results provide further evidence of the complexity of the molecular mechanism of follicular lipid dynamics during oogenesis in mosquitoes.

Introduction

Nutrient availability and their allocation towards life processes play a critical balance during insect life cycle.[1-3] For example, lipid allocation follows these trade decisions: female mosquitoes mobilized lipids towards the ovaries as a source of oocyte maturation while been also essential for energy homeostasis.[4-6] In *Aedes aegypti* mosquitoes, the ovary development and energy allocations during a gonotrophic cycle are typically divided in three major periods: previtellogenesis (PVG), ovarian resting stage (ORS) and vitellogenesis (VG).[7,8] Lipids and glycogen are the primary energy reserves for egg development during the immature stages.[5,9,10] These teneral reserves are partially consumed during the PVG period; moreover, nectar-feeding adds critical reserves during the ORS, and a blood meal triggers VG.[8,10-13] Previous studies revealed in *Aedes aegypti*, more than 80% of lipids found in eggs originate from sugars consumed before a blood meal.[14,15]

Sugar-feeding is a critical source of nutrients during the PVG stage. Sugar digestion starts in the crop, from which part of the meal is transferred periodically into the midgut (Figure 1).[16-18] Enzymes from the saliva ingested with the sugar meal and the midgut convert sucrose in glucose and fructose.[16,19] The biosynthesis of lipids begins in the midgut; sugars are used as precursors for fatty acid (FA) and triglycerides (TG) synthesis.[20,21] Experiments using radiolabeled sugars confirmed that they are utilized as substrate for TG synthesis.[22,23] While TG is the principal lipid produced in the fat body[24-26], most of the lipids found in the hemolymph are in the form of diglycerides (DG).[24,25,27] The transport of lipids among tissues is mediated by Lipophorin (Lp) and the Lipid Transfer Particle (LTP).[16,18,28,29] Previous studies suggested that the ovaries can only synthesize small amounts of lipids[30,31], therefore the majority of ovarian lipids must be produced elsewhere (e.g., fat body).[15,16,27,32]While TG reserves can be carried from the larva stage, *de novo* TG synthesis play undoubtedly a key role in *Ae. aegypti* oogenesis.[14,26,33]

In the present work, we studied ovarian TG dynamics during the PVG stage (2-7 days post-eclosion) of sugar-fed female *Ae. aegypti*. Stable isotopes from deuterated water were incorporated into the mosquito sugar diet, and TGs were detected using liquid chromatography coupled to Ultrahigh Resolution Mass Spectrometry (LC-UHRMS).[28,34-37] When a sugar diet with ^2H_2O was provided (Figure 1), *de novo* synthesized TGs were labeled with ^2H along the fatty

acyl tails. [38-40] This procedure permitted the identification of *de novo* synthesized TGs, as well as the analysis of the dynamics of ovary TG incorporation. A 14.5 T Fourier transform ion cyclotron resonance mass spectrometer (FT-ICR MS) equipped with hexapolar detection was utilized for effective isotope separation and chemical composition assignment. TGs were classified based on the fatty acid length and number of unsaturated bonds. Their relative abundances and degree of stable isotope incorporation (e.g., deuterium) were measured as a function of the time after adult eclosion.

Methods

Mosquito rearing conditions

Aedes aegypti of the Rockefeller strain were reared at 28 °C and 80% relative humidity. After eclosion, adult female mosquitoes were fed two different diet regimens: a) 20% Sucrose/ultrapure water (HPLC); b) 20% Sucrose/heavy water (^2H_2O). During the experiments, insects were fed daily by wetting a 1 × 1 inch cotton pad with each individual diet. Containers were loosely covered with polyethylene wrap to prevent rapid evaporation of the feeding pad.

Dissection and extraction of lipids

Female mosquitoes maintained on the two different diets were collected at different times after adult eclosion (2, 3, 4, 6 and 7 days) and immobilized by exposure to ice. Ovaries were dissected by performing an incision in the thorax, cutting the last abdominal segment and pulling out the ovaries.[27] Triplicates samples of 10 ovaries each were placed in 1.5 mL Eppendorf tubes, and 10 µL of a mix of labeled internal standard were added (EquiSplash Lipidomix, Avanti Polar Lipids, Alabaster, AL). After adding 100 µL of butanol/methanol and 3 µL of butylated hydroxytoluene, samples were homogenized for 10 seconds using polypropylene pestles (Fisher Scientific, Pittsburgh, PA), and a handheld cordless motor. The pestles were then rinsed with 200 µL of butanol/methanol. All tubes were sonicated for 30 minutes, and then centrifuged for 10 minutes. The supernatant was transferred into autosampler vials with 300 µL silanized glass inserts (Thermo Fisher Scientific, Waltham, MA).

LC-FT-ICR MS analysis

Lipid identification and quantitation were performed at the National High Magnetic Field Laboratory (Florida State University, Tallahassee, FL), using a 14.5 T Fourier-transform ion cyclotron resonance Mass Spectrometer (FT-ICR-MS) equipped with a hexapolar detection (3W+) system. The instrument is a hybrid linear quadrupole ion trap/FT-ICR MS (LTQ-FT, Thermo Fisher Corp., Bremen, Germany), adapted to operate in an actively shielded 14.5 T superconducting magnet (Magnex, Oxford, U.K.). Analysis were performed in positive ion mode, using an electrospray ionization (ESI) source, operating at 3.9 kV capillary voltage and 325 °C capillary temperature. All data were processed using an in-house software. The experimental MS resolving power was $m/Dm_{50\%}$ > 1000000 at m/z 800. The 14.5 T FT-ICR MS was coupled to a Waters e2695 Alliance HPLC system, equipped with an Accucore C_{30} column (Thermo Fisher Scientific, Sunnyvale, CA). Separations were done using acetonitrile (ACN), water (H_2O) and isopropanol (IPA). The phase A was a gradient with 30:40:30 (ACN:H_2O:IPA) and phase B was 10:5:85 (ACN:H2O:IPA). Both phases contained 10 mM ammonium acetate and 0.1% formic acid. HPLC conditions were an injection volume of 5 µL, solvent flow rate of 0.25 mL/min and 60 minutes of total run. The lipid intensity was normalized by the absolute intensity of the deuterated internal standard. The quantification was calculated based on the ratio between concentrations of the ovarian lipid species and internal standard. Standard error (± SE) was calculated between triplicate samples of 10 ovaries each.

Results

De novo synthesis of ovarian lipid reserves.

The use of stable isotope labelling combined with ultrahigh resolution mass spectrometry has shown significant advantages for the analysis of biological pathways.[6,26,28,41,42] Different from other labelling techniques, the incorporation of stable isotopes does not change the chemical properties of the lipid and allows the detection of the labeled molecule by their isotopic profile. This approach enables direct analysis of nutrient distribution, mobilization and metabolism.[4,23,37,43-45] While the concept is simple, for the analysis of complex biological samples it requires: i) the use of complementary pre-separation techniques to diminish matrix effects and increase the sensitivity of the analysis [27,37,46-53] and ii) the use of high magnetic fields to achieve ultrahigh mass resolution with short transient duration for compatibility with LC separation (e.g., resolving power greater than $m/Dm_{50\%}$ > 1000000 and mass accuracy better than 1 ppm).[27,36,41-43,46-48] More recently, in addition to the use of higher magnetic fields, alternative detection strategies (e.g., hexapolar detection, 3W+) has allowed better sensitivity and shorter analysis time, making more efficient the coupling of LC-FT-ICR MS.[41,46,47,54] Adult female mosquitoes were offered either 20% sucrose/water or 20% sucrose/^2H_2O water for a period of 2, 3, 4, 6 and 7 days after emergence. Inclusion of deuterated water (^2H_2O) in the mosquito diet during the PVG stage, provided unequivocal identification of *de novo* TG dynamics. When offered a sucrose-^2H_2O diet, adult female mosquitoes synthesized *de novo* FA using isotopically labeled substrates, such as acetyl CoA, NADPH and water, which became metabolically enriched with ^2H (Figure 1).

Identification and quantification of TGs from mosquito ovaries

Typical LC and MS profiles for unlabeled TGs extracted from ovaries generated using the LC-URMS workflow are shown in Figure 2. TG signals were in the 800-900 m/z range, eluting at 35-45 minutes after injection of the sample. The molecular ammonium adduct ion forms ($[M+NH_4]^+$) of TG species showed higher abundance than the sodium adduct ions ($[M+Na]^+$), and were used for quantitation analysis (Figure 2). In most cases, a single LC band was observed per TG; however, in the case of TG 50:4 and TG 50:5, the double bands corresponded to the presence of positional isomers. Table 1 displays a summary of the TGs detected using LC-FT-ICR MS with a mass accuracy lower than 300 ppb. TGs extracted from ovaries of females fed ^2H_2O labeled sugar diets revealed similar EIC profiles; although, the addition of ^2H creates distinct isotopic patterns (Figure S1). The use of ultrahigh resolution FT-ICR MS allowed the observance of the isotopic fine structure. This permits direct discrimination of the signals containing ^2H from that of naturally occurring isotopes (e.g., ^{13}C).

The *de novo* synthesized TGs have the characteristic presence of ^2H in their elemental composition (Figure 3). For example, the mass profile of *de novo* synthesized TG 48:2 showed the substitution of 30 hydrogens by deuterium atoms (Figure 3A). These substitutions were absent in ovarian samples from females that received a non-labeled sucrose diet (Figure 3B). A closer inspection to the 820 – 834 m/z range highlights the importance of ultrahigh resolution MS for this type of analysis (Figure 3C). For example, at the nominal mass level, the 826.70 – 826.80 range contains signals from TG 48:2 $[M+Na^+]$ $1x^{13}C$ isotope, TG 48:2 $[M+NH_4^+]$ $5x^2H$ and $1x^{13}C$ isotopes, and TG 48:2 $[M+NH_4^+]$ with $6x^2H$. These signals measured at lower resolving powers would result in convolution of the two peaks, contributing ambiguous peak assignment and spurious quantification values.

The trends of changes and quantities of TG were similar in ovaries from females raised on non-labeled diet and labeled diet (Figure 4). In good agreement with previous reports, TGs containing 48, 50, 52, and 54 carbons were the most abundant species.[27] As a general tendency, the amount of TGs increased with the days after eclosion, reaching a steady state towards the last days. Most significantly, deuterium incorporation was observed in all TGs species, but with unique dynamics for each of them. In terms of total lipid amounts, three-quarters of TG lipids were labeled during the six-day experiment, with the percentage of ^{2}H incorporation increasing as a function of time (Figures 4 and S2).

Dynamics of de novo TG incorporation into the ovary

The investigation of the dynamic changes of ovarian lipids during the PVG period was assisted by the incorporation of stable isotopes, providing an additional dimension of absolute quantitative values. The analysis of the number of deuterium atoms incorporated into eighteen different TG species at different days after adult eclosion, indicated a dynamic constant adjustment of ovarian TG stores during the experiment. In Figure 5, we display the distribution of the number of deuterium incorporated into each TG as a function of time. Results are expressed as amount of ovarian TG deuterated species relative to the TG 48:1 (d7) internal standard using a color scale. The replacement of hydrogen by deuterium in TGs was already detected at day 2 after eclosion. At day 3 we observed a significant increase of ^{2}H-TGs. The day when we recorded the highest number of incorporated ^{2}H was different depending on the carbon number and unsaturation degree of the TG. At day 4, TGs 54:2, 54:5 and 54:6 have at least 20x ^{2}H incorporated into their lipid chains; while TG 50:4, TG 52:1 and TG 52:2 have less than 10x ^{2}H incorporated. We observed a positive correlation between the number of ^{2}H incorporated into a TG and the carbon number, molecular size and number of unsaturated bonds. TG 54 and TG 52 were more abundant than TG 48, validating a relation between chain length and ability to incorporate deuterium. Interestingly, at day 7 the median number of ^{2}H incorporations and total amount of TGs species in the ovary decreased; except for TGs 52:3, 52:4 and 52:5, suggesting that some of the follicles might have been resorbed. In terms of kinetics, the saturated species, such as TG 50:1; TG 52:1; TG 54:2, showed high deuterium incorporation at day 3, suggesting the deuteriums incorporated in single bonds are more stable than those incorporated in species rich in double bonds, such as TG 50:5; TG 52:5 and TG 54:6.

Discussion

Oogenesis is energetically costly. *Ae. aegypti* females can lay over 120 eggs in a gonotrophic cycle; therefore, a tightly regulated control of nutrient allocations to the ovaries is critical.[5,7,8,10,27] The ovarian resting stage in *Ae. aegypti*, is a period marked by constant adjustment of the reproductive output based on nutritional and hormonal status; this adjustment typically occurs through follicular resorption by apoptosis.[5,7,30] The link between an increased oocyte lipid content and a successful reproductive output has been reported in invertebrate and vertebrate systems.[11,13,23] In this study, we started to address a fundamental question: “Can we use stable isotopes to establish time profiles of TGs incorporation into the developing ovarian follicles (composition, abundance and dynamic changes), which could lead us to a better understanding on the effect of nutrients on the dynamic importation of follicular lipids during oogenesis? “

In the current experiments we focused in addressing the issue of the distinct contributions of teneral reserves (those already carried at adult eclosion) and adult sugar feeding to the TGs imported into the ovarian follicles during the previtellogenic stage. To discriminate between these two nutritional sources, we labeled the lipids that were *de novo*

synthesized using a $^{2}H_2O$ labeled sugar diet. Taking the advantage of stable isotope labelling; our studies confirmed that a significant portion of the ovary lipids were isotopically labeled with ^{2}H, indicating an active *de novo* TG synthesis and transport into the ovaries. The dynamic changes on the ovarian TG lipid profiles suggested that ovarian TG lipids were utilized and replaced by *de novo* synthesized lipids. An increase of ^{2}H-labelling was correlated with increases in carbon number, molecular size, and number of unsaturated bonds of TGs. Overall, the replacement of hydrogen atoms by deuterium is also influence by enzymatic activities and kinetic parameters. Based on lipids dynamics, labeled ^{2}H-TGs were incorporated into the ovaries during the entire experiment, but the total lipid amount was either reduced or stable by day 7, suggesting that some of the follicles might have been resorbed.

In summary, our studies showed *de novo* TG lipid mobilization and storage into the developing ovaries. The use of a stable isotope labeled-sugar diet enabled the dynamic study of lipid incorporation into ovarian follicles at the TG species level. The LC-UHRMS workflow provides the isotopic profile of characteristic TG species and the number of deuterium incorporated. Multiple TG species were detected in the 800 to 900 m/z range with a mass accuracy lower than 300 ppb. Non-labeled diets and labeled diets promoted similar quantities of TG lipids to be transferred to the ovaries. Despite the existence of a significant amount of lipid teneral reserves, TGs were synthetized *de novo* from the second day after adult emergence, and rapidly stored in the oocytes. An overall rise in *de novo* TG synthesis was observed for all TG species, with increases over time in the chain length sizes and number of unsaturated bonds of labelled TGs. The kinetics of label incorporation over time supports the idea that ovarian lipids are consumed or recycled during the PVG stage. Future studies using additional stable isotope (e.g., ^{13}C) and complementary TG measurements from other mosquito tissue compartments (e.g., hemolymph, fat body, etc.) can provide further information about the TG allocation and mobilization in and out of the ovaries during the PVG stage.

Declarations

Acknowledgements

This work was supported by the NIH grant No. R21AI135469 to FFL and R01AI04554 to FGN. A portion of this work was performed at the National High Magnetic Field Laboratory ICR User Facility, which is supported by the National Science Foundation Division of Chemistry through DMR-1644779 and the State of Florida.

Author contributions statement

Conception of the study: F.G.N. and F.F.L. Sample preparation: L.V.T, V.M. and M.N. Data collection: L.V.T. and C.R.W. Data analysis and interpretation: L.V.T., C.R.W., V.M., M.N., F.G.N. and F.F.L. Manuscript writing and figures: L.V.T., F.G.N. and F.F.L. All authors reviewed the manuscript.

Corresponding Author

*Corresponding authors: Francisco A. Fernández-Lima, Department of Chemistry and Biochemistry, Florida International University, 11200 SW 8th St AHC4-233, Miami, FL 33199, USA;

e-mail: fernandf@fiu.edu.

Competing interests

The authors declare no competing financial interest.

References

1. Boggs, C. L. Resource-Allocation - Exploring Connections between Foraging and Life-History. *Funct Ecol.* **6**, 508–518 doi:Doi 10.2307/2390047 (1992).
2. Stevens, D. J., Hansell, M. H. & Monaghan, P. Developmental trade-offs and life histories: strategic allocation of resources in caddis flies. *P Roy Soc B-Biol Sci.* **267**, 1511–1515 (2000).
3. Wheeler, D. The role of nourishment in oogenesis. *Annual Review of Entomology.* **41**, 407–431 (1996).
4. Hoc, B. *et al.* About lipid metabolism in Hermetia illucens (L. 1758): on the origin of fatty acids in prepupae.*Sci Rep-Uk***10** (2020).
5. Caroci, A. S., Li, Y. & Noriega, F. G. Reduced juvenile hormone synthesis in mosquitoes with low teneral reserves reduces ovarian previtellogenic development in Aedes aegypti. *J Exp Biol.* **207**, 2685–2690 https://doi.org/10.1242/jeb.01093 (2004).
6. Oliveira, G. A. *et al.* Flight-oogenesis syndrome in a blood-sucking bug: biochemical aspects of lipid metabolism. *Arch Insect Biochem Physiol.* **62**, 164–175 https://doi.org/10.1002/arch.20132 (2006).
7. Clifton, M. E. & Noriega, F. G. Nutrient limitation results in juvenile hormone-mediated resorption of previtellogenic ovarian follicles in mosquitoes. *Journal of insect physiology.* **57**, 1274–1281 https://doi.org/10.1016/j.jinsphys.2011.06.002 (2011).
8. Noriega, F. G. Juvenile Hormone Biosynthesis in Insects: What Is New, What Do We Know, and What Questions Remain? Int Sch Res Notices 2014, 967361 (2014).
9. Ramirez, C. E. *et al.* Fast, ultra-trace detection of juvenile hormone III from mosquitoes using mass spectrometry. *Talanta.* **159**, 371–378 https://doi.org/10.1016/j.talanta.2016.06.041 (2016).
10. Noriega, F. G. Nutritional regulation of JH synthesis: a mechanism to control reproductive maturation in mosquitoes? *Insect biochemistry and molecular biology.* **34**, 687–693 https://doi.org/10.1016/j.ibmb.2004.03.021 (2004).
11. Briegel, H. Mosquito Reproduction - Incomplete Utilization of the Blood Meal Protein for Oogenesis. *Journal of insect physiology.* **31**, 15–21 doi:Doi 10.1016/0022-1910(85)90036-8 (1985).
12. Klowden, M. J. Endocrine aspects of mosquito reproduction. *Arch Insect Biochem.* **35**, 491–512 (1997).
13. Clifton, M. E. & Noriega, F. G. The fate of follicles after a blood meal is dependent on previtellogenic nutrition and juvenile hormone in Aedes aegypti. *Journal of insect physiology.* **58**, 1007–1019 https://doi.org/10.1016/j.jinsphys.2012.05.005 (2012).
14. Zhou, G., Pennington, J. E. & Wells, M. A. Utilization of pre-existing energy stores of female Aedes aegypti mosquitoes during the first gonotrophic cycle. *Insect biochemistry and molecular biology.* **34**, 919–925 https://doi.org/10.1016/j.ibmb.2004.05.009 (2004).
15. Wang, X. L. *et al.* Hormone and receptor interplay in the regulation of mosquito lipid metabolism. *P Natl Acad Sci USA.* **114**, E2709–E2718 https://doi.org/10.1073/pnas.1619326114 (2017).
16. Foster, W. A. Mosquito sugar feeding and reproductive energetics. *Annu Rev Entomol.* **40**, 443–474 https://doi.org/10.1146/annurev.en.40.010195.002303 (1995).
17. Gill, M., Thornley, J. H., Black, J. L., Oldham, J. D. & Beever, D. E. Simulation of the metabolism of absorbed energy-yielding nutrients in young sheep. *Br J Nutr.* **52**, 621–649 https://doi.org/10.1079/bjn19840129 (1984).
18. Louie, K. B. *et al.* Mass spectrometry imaging for in situ kinetic histochemistry. *Sci Rep-Uk* **3**, doi:ARTN 1656 10.1038/srep01656 (2013).

19. Chino, H. & Gilbert, L. I. Diglyceride Release from Insect Fat Body: A Possible Means of Lipid Transport. *Science.* **143**, 359–361 https://doi.org/10.1126/science.143.3604.359 (1964).
20. Inagaki, S. & Yamashita, O. Metabolic Shift from Lipogenesis to Glycogenesis in the Last Instar Larval Fat-Body of the Silkworm, Bombyx-Mori. *Insect Biochem.* **16**, 327–331 (1986).
21. Hill, S., Winning, B., Jenner, H., Knorpp, C. & Leaver, C. Role of NAD(+)-dependent 'malic' enzyme and pyruvate dehydrogenase complex in leaf metabolism. *Biochem Soc T.* **24**, 743–746 https://doi.org/10.1042/bst0240743 (1996).
22. Ziegler, R. & Ibrahim, M. M. Formation of lipid reserves in fat body and eggs of the yellow fever mosquito, Aedes aegypti. *Journal of insect physiology.* **47**, 623–627 https://doi.org/10.1016/s0022-1910(00)00158-x (2001).
23. Briegel, H. Metabolic Relationship between Female Body Size, Reserves, and Fecundity of Aedes-Aegypti. *Journal of insect physiology.* **36**, 165–172 doi:Doi 10.1016/0022-1910(90)90118-Y (1990).
24. Hagedorn, H. H. *et al.* Postemergence growth of the ovarian follicles of Aedes aegypti. *Journal of insect physiology.* **23**, 203–206 (1977).
25. Clements, A. N. & Clements, A. N. *The biology of mosquitoes* 1st edn (Chapman & Hall Cambridge, MA CABI, 1992).
26. Zhou, G. *et al.* Metabolic fate of [14C]-labeled meal protein amino acids in Aedes aegypti mosquitoes. *Journal of insect physiology.* **50**, 337–349 https://doi.org/10.1016/j.jinsphys.2004.02.003 (2004).
27. Castellanos, A. *et al.* Three Dimensional Secondary Ion Mass Spectrometry Imaging (3D-SIMS) of Aedes aegypti ovarian follicles. *J Anal At Spectrom.* **34**, 874–883 https://doi.org/10.1039/C8JA00425K (2019).
28. Guo, Z. K., Cella, L. K., Baum, C., Ravussin, E. & Schoeller, D. A. De novo lipogenesis in adipose tissue of lean and obese women: application of deuterated water and isotope ratio mass spectrometry. *Int J Obesity.* **24**, 932–937 https://doi.org/10.1038/sj.ijo.0801256 (2000).
29. McEvoy, T. G., Coull, G. D., Broadbent, P. J., Hutchinson, J. S. & Speake, B. K. Fatty acid composition of lipids in immature cattle, pig and sheep oocytes with intact zona pellucida. *Journal of reproduction and fertility.* **118**, 163–170 (2000).
30. Ziegler, R. Lipid synthesis by ovaries and fat body of Aedes aegypti (Diptera: Culicidae). *Eur J Entomol.* **94**, 385–391 (1997).
31. Brunelle, A., Touboul, D. & Laprevote, O. Biological tissue imaging with time-of-flight secondary ion mass spectrometry and cluster ion sources. *Journal of Mass Spectrometry.* **40**, 985–999 https://doi.org/10.1002/jms.902 (2005).
32. Wang, Q. & Sun, Q. Y. Evaluation of oocyte quality: Morphological, cellular and molecular predictors. *Reprod Fert Develop.* **19**, 1–12 https://doi.org/10.1071/RD06103 (2007).
33. Dunning, K. R., Russell, D. L. & Robker, R. L. Lipids and oocyte developmental competence: the role of fatty acids and beta-oxidation. *Reproduction (Cambridge, England).* **148**, R15–27 (2014).
34. Adams, K. J., Montero, D., Aga, D. & Fernandez-Lima, F. Isomer separation of polybrominated diphenyl ether metabolites using nanoESI-TIMS-MS. *Int J Ion Mobil Spec.* **19**, 69–76 https://doi.org/10.1007/s12127-016-0198-z (2016).
35. Armbrecht, L. & Dittrich, P. S. Recent Advances in the Analysis of Single Cells. *Anal Chem.* **89**, 2–21 https://doi.org/10.1021/acs.analchem.6b04255 (2017).
36. Benigni, P., Thompson, C. J., Ridgeway, M. E., Park, M. A. & Fernandez-Lima, F. Targeted high-resolution ion mobility separation coupled to ultrahigh-resolution mass spectrometry of endocrine disruptors in complex

mixtures. *Anal Chem.* **87**, 4321–4325 https://doi.org/10.1021/ac504866v (2015).

37. Khalil, S. M., Rompp, A., Pretzel, J., Becker, K. & Spengler, B. Phospholipid Topography of Whole-Body Sections of the Anopheles stephensi Mosquito, Characterized by High-Resolution Atmospheric-Pressure Scanning Microprobe Matrix-Assisted Laser Desorption/Ionization Mass Spectrometry Imaging. *Anal Chem.* **87**, 11309–11316 (2015).
38. Tsugawa, H. *et al.* A lipidome atlas in MS-DIAL 4. *Nat Biotechnol.* **38**, 1159–1159 https://doi.org/10.1038/s41587-020-0531-2 (2020).
39. Tsugawa, H. *et al.* MS-DIAL: data-independent MS/MS deconvolution for comprehensive metabolome analysis. *Nat Methods.* **12**, 523–526 https://doi.org/10.1038/nmeth.3393 (2015).
40. Onjiko, R. M., Moody, S. A. & Nemes, P. Single-cell mass spectrometry reveals small molecules that affect cell fates in the 16-cell embryo. *Proc Natl Acad Sci U S A.* **112**, 6545–6550 https://doi.org/10.1073/pnas.1423682112 (2015).
41. Samarah, L. Z. *et al.* Single-Cell Metabolic Profiling: Metabolite Formulas from Isotopic Fine Structures in Heterogeneous Plant Cell Populations. *Anal Chem.* **92**, 7289–7298 https://doi.org/10.1021/acs.analchem.0c00936 (2020).
42. Trotzmuller, M. *et al.* Determination of the Isotopic Enrichment of (13)C- and (2)H-Labeled Tracers of Glucose Using High-Resolution Mass Spectrometry: Application to Dual- and Triple-Tracer Studies. *Anal Chem.* **89**, 12252–12260 https://doi.org/10.1021/acs.analchem.7b03134 (2017).
43. Leaptrot, K. L., May, J. C., Dodds, J. N. & McLean, J. A. Ion mobility conformational lipid atlas for high confidence lipidomics. *Nat Commun.* **10**, 985 https://doi.org/10.1038/s41467-019-08897-5 (2019).
44. Shi, L. Y. *et al.* Optical imaging of metabolic dynamics in animals.*Nat Commun***9** (2018).
45. Tejedor, M. L., Mizuno, H., Tsuyama, N., Harada, T. & Masujima, T. In Situ Molecular Analysis of Plant Tissues by Live Single-Cell Mass Spectrometry. *Anal Chem.* **84**, 5221–5228 https://doi.org/10.1021/ac202447t (2012).
46. Ruddy, B. M., Blakney, G. T., Rodgers, R. P., Hendrickson, C. L. & Marshall, A. G. Elemental composition validation from stored waveform inverse Fourier transform (SWIFT) isolation FT-ICR MS isotopic fine structure. *J Am Soc Mass Spectrom.* **24**, 1608–1611 https://doi.org/10.1007/s13361-013-0695-9 (2013).
47. Schaub, T. M. *et al.* High-performance mass spectrometry: Fourier transform ion cyclotron resonance at 14.5 Tesla. *Anal Chem.* **80**, 3985–3990 https://doi.org/10.1021/ac800386h (2008).
48. Benigni, P. & Fernandez-Lima, F. Oversampling Selective Accumulation Trapped Ion Mobility Spectrometry Coupled to FT-ICR MS: Fundamentals and Applications. *Anal Chem.* **88**, 7404–7412 (2016).
49. Lanni, E. J., Dunham, S. J., Nemes, P., Rubakhin, S. S. & Sweedler, J. V. Biomolecular imaging with a C60-SIMS/MALDI dual ion source hybrid mass spectrometer: instrumentation, matrix enhancement, and single cell analysis. *J Am Soc Mass Spectrom.* **25**, 1897–1907 https://doi.org/10.1007/s13361-014-0978-9 (2014).
50. Pan, N., Rao, W., Standke, S. J. & Yang, Z. B. Using Dicationic Ion-Pairing Compounds To Enhance the Single Cell Mass Spectrometry Analysis Using the Single-Probe: A Microscale Sampling and Ionization Device. *Anal Chem.* **88**, 6812–6819 (2016).
51. Piwowar, A. M. *et al.* C60-ToF SIMS imaging of frozen hydrated HeLa cells. *Surf Interface Anal.* **45**, 302–304 (2013).
52. Rao, W., Pan, N. & Yang, Z. B. High Resolution Tissue Imaging Using the Single-probe Mass Spectrometry under Ambient Conditions. *J Am Soc Mass Spectrom.* **26**, 986–993 (2015).

53. Rao, W., Pan, N. & Yang, Z. B. Applications of the Single-probe: Mass Spectrometry Imaging and Single Cell Analysis under Ambient Conditions.*Jove-J Vis Exp*(2016).
54. Cho, E., Witt, M., Hur, M., Jung, M. J. & Kim, S. Application of FT-ICR MS Equipped with Quadrupole Detection for Analysis of Crude Oil. *Anal Chem.* **89**, 12101–12107 https://doi.org/10.1021/acs.analchem.7b02644 (2017).

Table

Table 1. LC-FT-ICR MS triglyceride assignments for ovarian TG 48, TG 50, TG 52 and TG 54.

Lipid	Neutral formula	$[M+NH_4]^+$	Theoretical Mass	Experimental Mass	Retention time (min)	Error (ppm)
TG 15:0/18:1(d7)/15:0	$C_{51}H_{89}O_6D_7$	$[C_{51}H_{89}O_6D_7+NH_4]^+$	829.798454	829.79840	39.1-40.1	0.065
TG 48:3	$C_{51}H_{92}O_6$	$[C_{51}H_{92}O_6+NH_4]^+$	818.723216	818.72272	37.9-38.1	0.124
TG 48:2	$C_{51}H_{94}O_6$	$[C_{51}H_{94}O_6+NH_4]^+$	820.738866	820.73840	38.1-39.1	0.136
TG 48:1	$C_{51}H_{96}O_6$	$[C_{51}H_{96}O_6+NH_4]^+$	822.754516	822.75418	39.6-40.3	0.109
TG 50:5	$C_{53}H_{92}O_6$	$[C_{53}H_{92}O_6+NH_4]^+$	842.723216	842.72303	36.2-37.3	0.229
TG 50:4	$C_{53}H_{94}O_6$	$[C_{53}H_{94}O_6+NH_4]^+$	844.738866	844.73854	37.1-38.2	0.440
TG 50:3	$C_{53}H_{96}O_6$	$[C_{53}H_{96}O_6+NH_4]^+$	846.754516	846.75406	38.2-39.0	0.320
TG 50:2	$C_{53}H_{98}O_6$	$[C_{53}H_{98}O_6+NH_4]^+$	848.770166	848.76999	39.7-40.5	0.250
TG 50:1	$C_{53}H_{100}O_6$	$[C_{53}H_{100}O_6+NH_4]^+$	850.785816	850.78554	41.2-42.0	0.153
TG 52:5	$C_{55}H_{96}O_6$	$[C_{55}H_{96}O_6+NH_4]^+$	870.754516	870.75429	38.0-38.6	0.180
TG 52:4	$C_{55}H_{98}O_6$	$[C_{55}H_{98}O_6+NH_4]^+$	872.770166	872.77004	38.6-39.7	0.245
TG 52:3	$C_{55}H_{100}O_6$	$[C_{55}H_{100}O_6+NH_4]^+$	874.785816	874.78548	39.7-40.4	0.105
TG 52:2	$C_{55}H_{102}O_6$	$[C_{55}H_{102}O_6+NH_4]^+$	876.801466	876.80114	41.3-42.1	0.120
TG 52:1	$C_{55}H_{104}O_6$	$[C_{55}H_{104}O_6+NH_4]^+$	878.817116	878.81682	43.1-43.7	0.245
TG 54:6	$C_{57}H_{98}O_6$	$[C_{57}H_{98}O_6+NH_4]^+$	896.770166	896.77020	38.1-38.5	0.175
TG 54:5	$C_{57}H_{100}O_6$	$[C_{57}H_{100}O_6+NH_4]^+$	898.785816	898.546	38.8-39.5	0.109
TG 54:4	$C_{57}H_{102}O_6$	$[C_{57}H_{102}O_6+NH_4]^+$	900.801466	900.80103	40.0-40.4	0.350
TG 54:3	$C_{57}H_{104}O_6$	$[C_{57}H_{104}O_6+NH_4]^+$	902.817116	902.81693	41.2-41.7	0.240
TG 54:2	$C_{57}H_{106}O_6$	$[C_{57}H_{106}O_6+NH_4]^+$	904.832766	904.83222	43.0-44.2	0.170

Figures

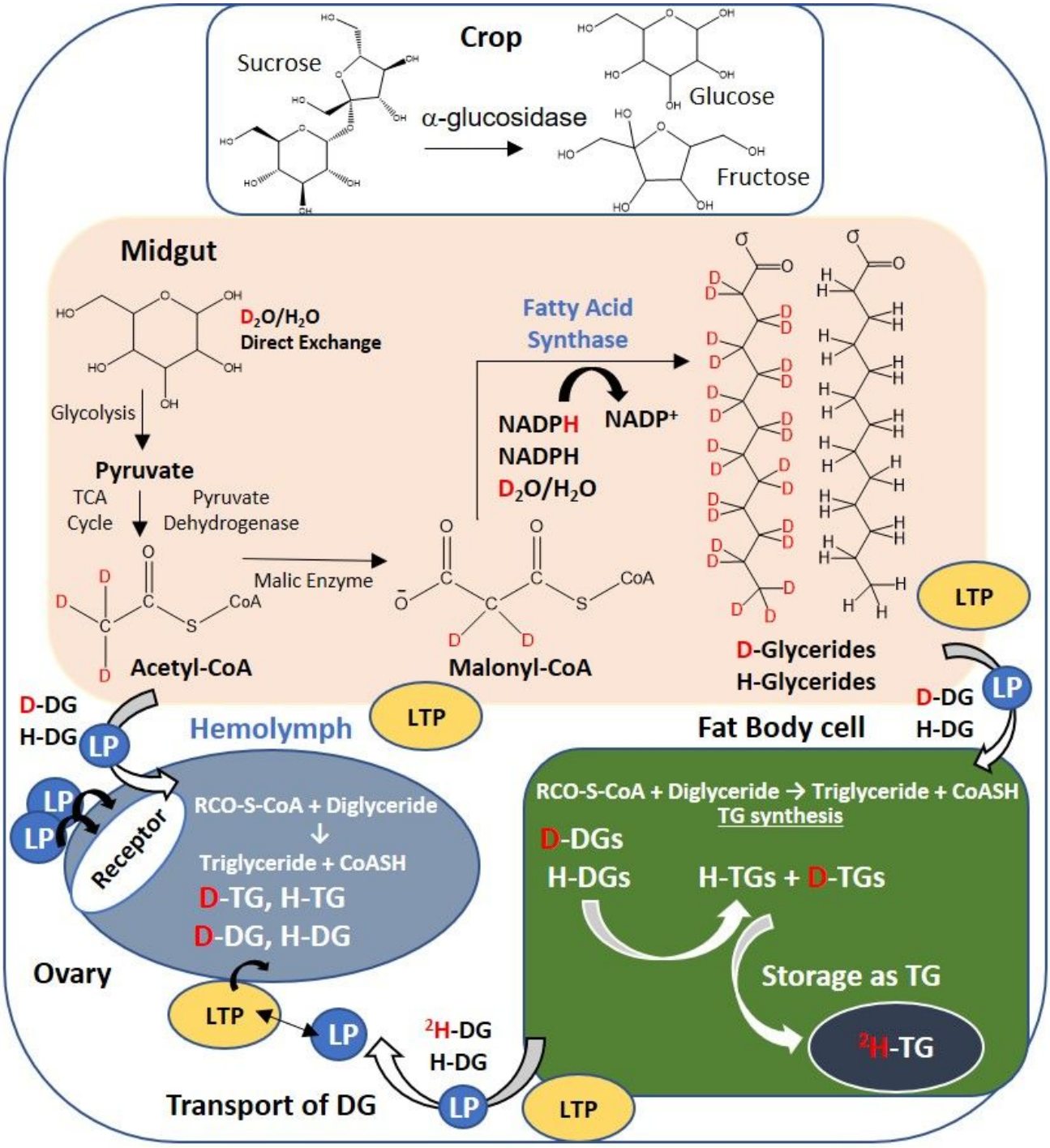

Figure 1

Deuterium incorporation into triglycerides occurs during de novo fatty acid synthesis. Different tissue compartments are represented (crop, midgut, hemolymph, ovary and fat body). The TG synthetic pathway utilizes substrates that have been labelled with deuterium, including acetyl CoA, NADPH and water. Hydrogen atoms (H) highlighted in red indicate the location where deuterium (D) may have replaced hydrogen in a newly synthesized molecule. TCA cycle: tricarboxylic acid cycle. CoASH: coenzyme A. RCO-S-CoA: acetyl-coenzyme A. Malonyl-CoA: malonyl coenzyme A. NADPH: nicotinamide adenine dinucleotide phosphate. LTP: lipid transfer particle. LP: lipophorin. DG: diglyceride. TG: triglyceride.

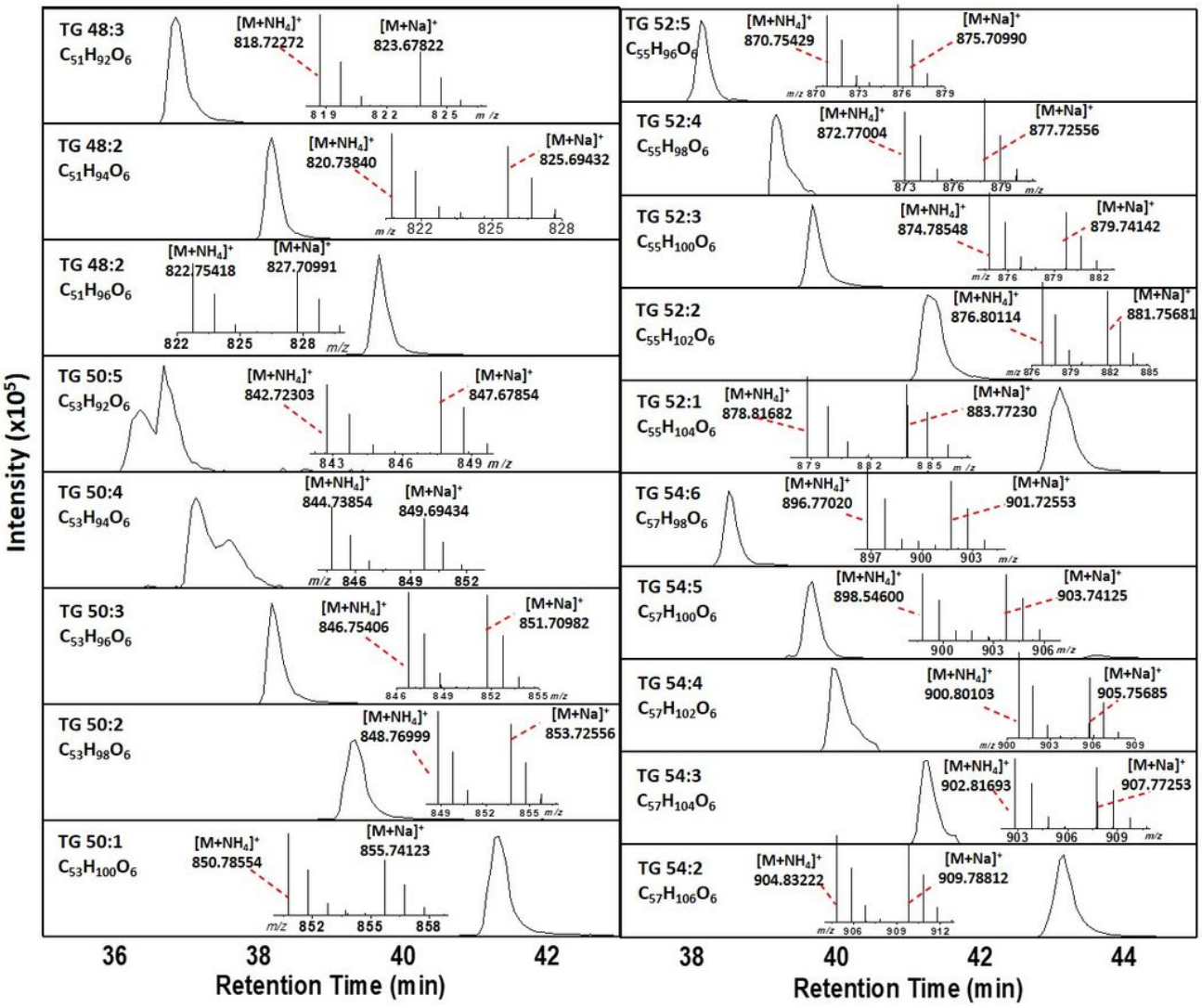

Figure 2

Extracted Ion Chromatograms of selected triglycerides species as ammonium ion form [M+NH4]+. The mass spectra is zooming on isotopic profiles for TGs in ammonium [M+NH4]+ and sodium [M+Na]+ ion forms.

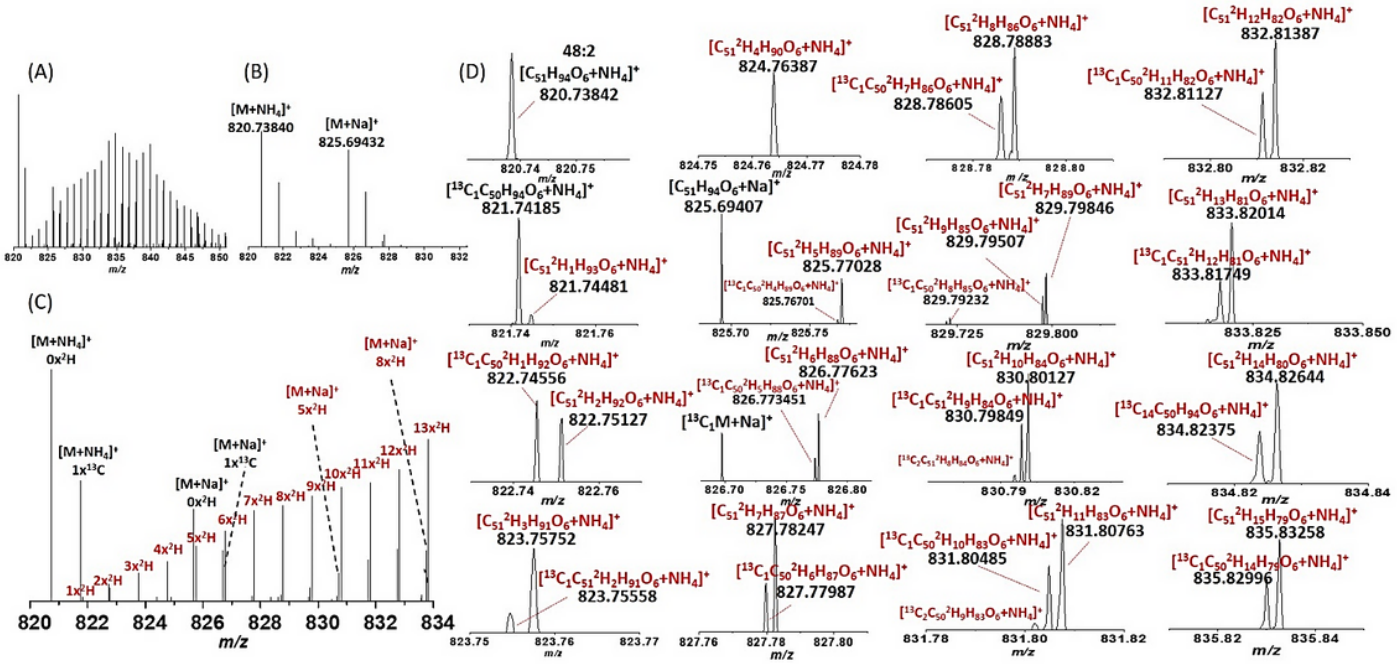

Figure 3

(A and B): Typical MS projections for the signal corresponding to 48:2 TG from ovarian samples. Deuterium labeled diet (A) and normal diets (B). Note the increase complexity of the MS signals with increases of the number of deuteriums incorporated and ion forms. (C and D): Amplified MS projections denoting the sources for isobaric interferences in the 820-834 m/z range, and the corresponding nominal masses. The TG species containing deuterium are highlighted in red.

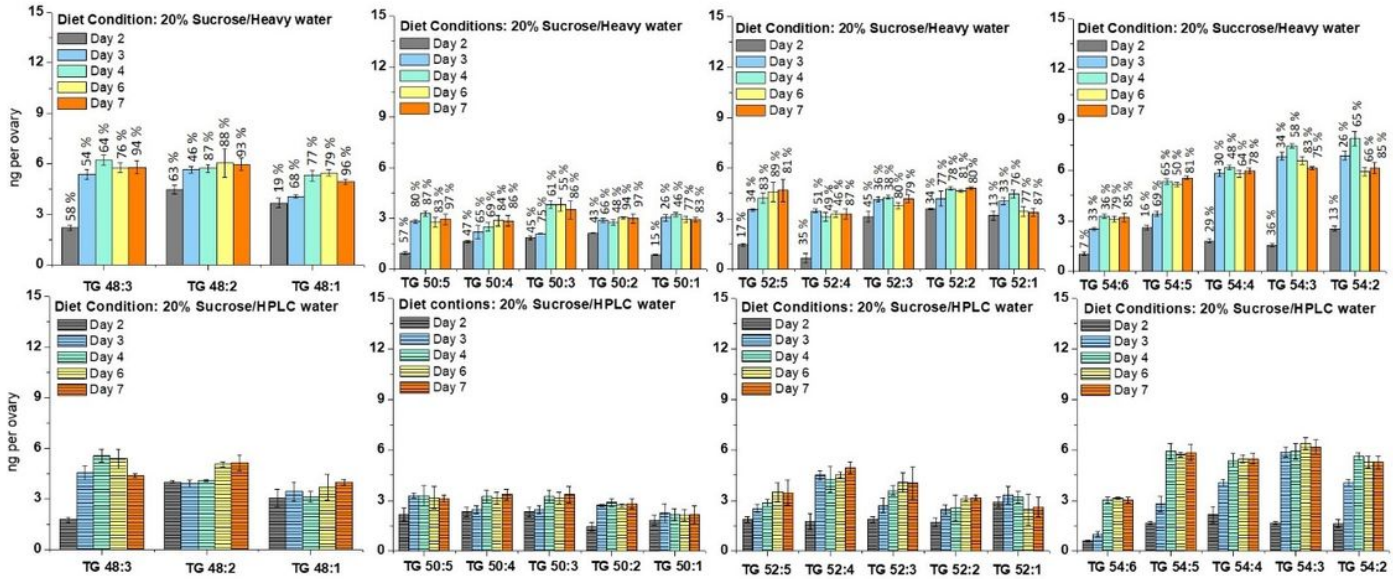

Figure 4

Quantitation of total amounts of different TG species in ovaries as a function of diet and time. Upper panel: 20% Sucrose/Heavy water diet. The numbers in the top are referring to the percentages of 2H incorporated into TGs.

Lower panel: 20% sucrose/HPLC water diet. Bars are means standard error (± SE) of the analysis of triplicates samples of 10 ovaries each.

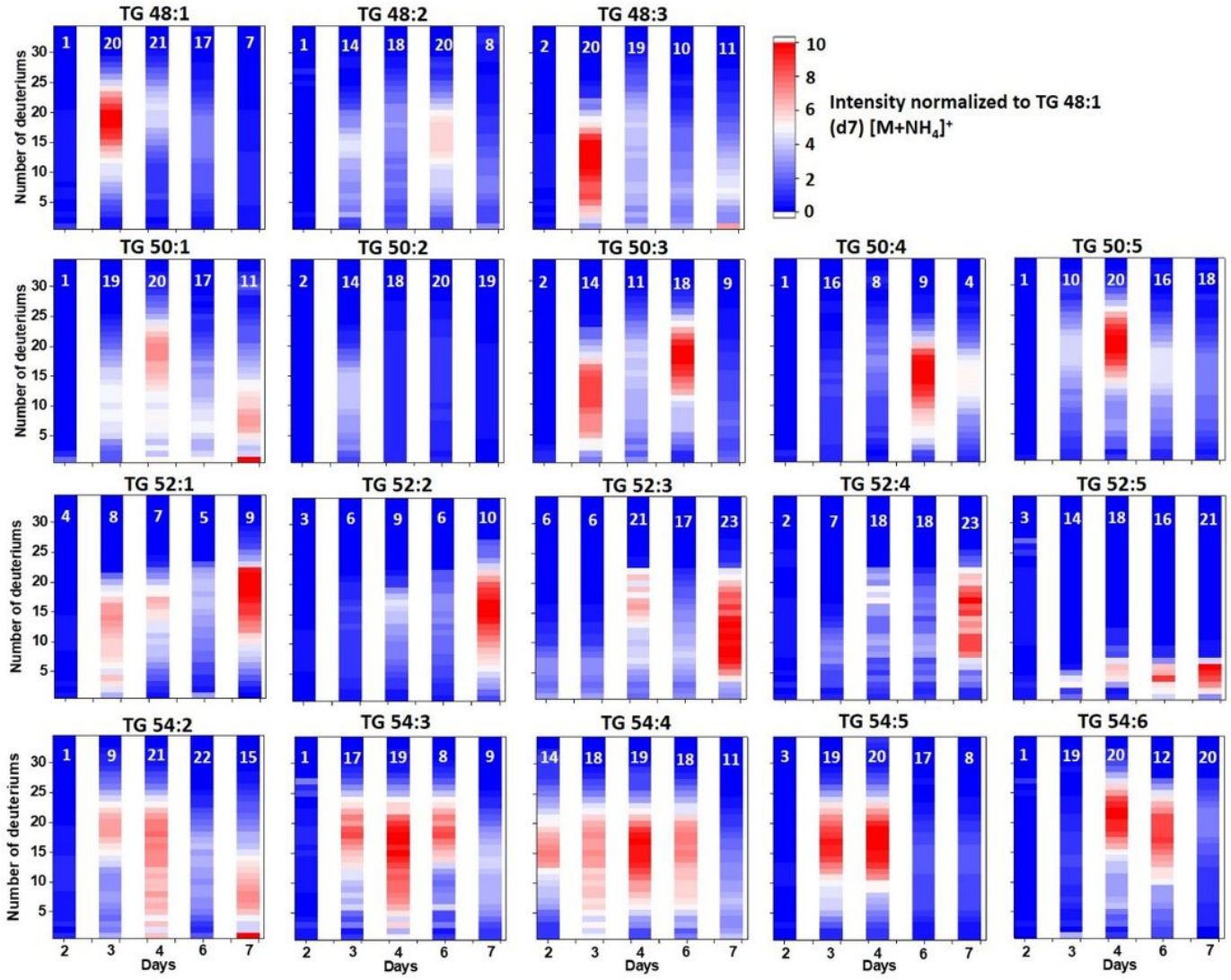

Figure 5

Distribution of the number of deuteriums per TG species as a function of days after eclosion (2-7 days). The median number of deuteriums is shown in the insets (white label). The color scale corresponds to the amount of deuterated species relative to the TG 48:1 (d7) internal standard.

Supplementary Files

This is a list of supplementary files associated with this preprint. Click to download.

- SupplementaryinformationV9.pdf